Journal of The Electrochemical Society, **155** (12) B1264-B1269 (2008)
0013-4651/2008/155(12)/B1264/6/$23.00 © The Electrochemical Society

An Oxide Ion and Proton Co-Ion Conducting $Sn_{0.9}In_{0.1}P_2O_7$ Electrolyte for Intermediate-Temperature Fuel Cells

Xilin Chen,[a] Chunsheng Wang,[a,*,z] E. Andrew Payzant,[b] Changrong Xia,[c] and Deryn Chu[d]

[a]*Department of Chemical and Biomolecular Engineering, University of Maryland, College Park, Maryland 20742, USA*
[b]*Materials Science and Technology Division, Oak Ridge National Laboratory, Oak Ridge, Tennessee 37831-6064, USA*
[c]*Department of Materials Science and Engineering, University of Science and Technology of China, Hefei, Anhui, 230026, China*
[d]*U.S. Army Research Laboratory, Sensors and Electronic Devices Directorate, Adelphi, Maryland 20783-1197, USA*

The ionic conductivity of $Sn_{0.9}In_{0.1}P_2O_7$ ceramic was investigated under various atmospheres within the temperature range of 130–230°C. Similar to mixed-conductive perovskite oxides at high temperatures (such as $SrCe_{0.95}Yb_{0.05}O_{3-\alpha}$,$La_{0.9}Sr_{0.1}Ga_{0.8}Mg_{0.2}O_{3-\alpha}$ at 600–1000°C), $Sn_{0.9}In_{0.1}P_2O_7$ can conduct both protons and oxide ions at low temperatures (130–230°C). The conductivity of $Sn_{0.9}In_{0.1}P_2O_7$ reaches 0.019 S/cm at 200°C in wet nitrogen. Its transport numbers determined by steam concentration cells are around 0.76 for a proton and 0.12 for an oxide ion. The performance of direct methanol fuel cells at 170°C using mixed-ion conductive $Sn_{0.9}In_{0.1}P_2O_7$ electrolyte is higher than that at 235°C using pure proton conductive CsH_2PO_4 electrolyte. This is attributed to direct oxidation of CO at the anode by the oxide ions generated at the cathode and moved through the $Sn_{0.9}In_{0.1}P_2O_7$ electrolyte.
 [DOI: 10.1149/1.2988135]

Manuscript submitted August 7, 2008; revised manuscript received August 28, 2008. Published October 7, 2008.

Recently, intermediate temperature solid state fuel cells, which are operated in the temperature range of 150–300°C, attracted widespread interest because of their higher CO tolerance, faster electrochemical reaction kinetics, and simpler thermal and water management as compared to proton exchange membrane fuel cells (PEMFCs). Because the working temperatures of intermediate temperature fuel cells (ITFCs) are lower than that of solid oxide fuel cells (SOFCs), ITFCs would allow the use of oxidation-resistant metallic alloys or even plastics as interconnect materials. They would also reduce the operating cost, increase the durability, extend the service life, and permit more frequent temperature and performance cycling.[1,2]

Many anhydrous proton conductors have been investigated as the electrolytes for intermediate temperature H_2/O_2 fuel cells, such as $CsHSO_4$,[3] CsH_2PO_4,[4-7] NH_4PO_3-based composites,[8-13] and indium-doped SnP_2O_7.[14-16] Although the CO tolerance of CsH_2PO_4 fuel cells operating above 230°C (the transition temperature from a low- to a high-conductive phase) is much better than PEMFCs operating at 80°C, it is still lower than SOFCs because the hydrocarbon fuels can be directly electro-oxidized by the oxide ions in SOFCs[17,18] and the operation temperatures (above 600°C) of SOFC are much higher than that of ITFCs. A method to enhance the CO tolerance of ITFCs is to use a proton and oxide ion co-ion conductive electrolyte membrane to replace the currently used proton conductive membrane. In such a cell, oxide ions are generated by the electrochemical reduction of dioxygen at the cathode and diffuse through the mixed oxide ion/proton membrane to the anode, where they may efficiently and directly oxidize any CO at the anode.

Most hydrocarbon oxidation reactions follow the Mars–van Krevelen mechanism,[19-22] in which surface lattice O^{2-} is the actual oxidation agent. During these reactions, the O^{2-} reactant plays two important roles: (*i*) being responsible for the removal of H from C–H bonds to give water as in oxidative dehydrogenation, and (*ii*) being capable of insertion into the intermediate complex to give the oxygenated product and water (mild oxidation). This mechanism is more efficient than that in the direct methanol fuel cell, in which methanol is directly electro-oxidized at low temperature by adsorbed hydroxide on a Pt–Ru electrocatalyst. It is the reason why an oxide-ion-conductive ceramic-supported Pt or Pt–Ru catalyst has a very high CO oxidation ability, even at low temperatures provided an oxygen (or oxide ion) source is present. It has been reported that $Sn_{0.9}In_{0.1}P_2O_7$ ITFCs can tolerate up to 10% CO in H_2; i.e., 10% CO added to H_2 at the anode did not decrease the performance of $Sn_{0.9}In_{0.1}P_2O_7$ ITFC at 250°C.[14,15] The excellent CO tolerance at the anode for $Sn_{0.9}In_{0.1}P_2O_7$ ITFCs may be attributed to the oxide ions transferring from the cathode through oxygen vacancies in $Sn_{0.9}In_{0.1}P_2O_7$ because of the existence of oxygen vacancies in $Sn_{0.9}In_{0.1}P_2O_7$.[14,16]

In this work, the proton and oxide ion co-ion conductivity of $Sn_{0.9}In_{0.1}P_2O_7$ and the performance of $Sn_{0.9}In_{0.1}P_2O_7$ fuel cells with methanol and/or hydrogen fuel were investigated. A fuel cell using a co-ion conducting $Sn_{0.9}In_{0.1}P_2O_7$ membrane, operating at temperatures of 170–200°C, combined the advantages of both the SOFC and PEMFC, and complemented existing proton and oxide-ion fuel cell systems. The goal of introducing oxide-ion transport in a proton conducting ceramic is to oxidize CO and methanol in an ITFC, which is different from prior works on mixed proton/oxide ion conducting perovskite oxides (such as $SrCe_{0.95}Yb_{0.05}O_{3-\alpha}$,[23] $La_{0.9}Sr_{0.1}Ga_{0.8}Mg_{0.2}O_{3-\alpha}$[24]), for which proton conductivity is thermally activated at a lower temperature than that required for oxide ion conduction[25] and hence enables a lower SOFC operating temperature.

Experimental

In^{3+}-doped SnP_2O_7 was prepared using SnO_2 (Sigma-Aldrich, 99.9%), In_2O_3 (Aldrich, 99.99%), and H_3PO_4 (Fisher Scientific, 85%) to form $Sn_{0.9}In_{0.1}P_2O_7$. The starting materials were mixed and held with stirring at 300°C until the mixture formed a paste with a high viscosity. The pastes were calcined at 650°C for 2.5 h and then ground into powders with a mortar and pestle. The compound was pressed at 250 MPa into pellets and then coated with Ag for conductivity measurement and with a Pt catalyst for fuel cell testing. The pellets were 13 mm in diameter and around 0.8 mm in thickness. For comparison, CsH_2PO_4 was also prepared as described in Ref. 4 using Cs_2CO_3 (Sigma-Aldrich 99%) and H_3PO_4 (Fisher Scientific 85%) as precursors. The crystalline structure of the compounds was analyzed by X-ray diffraction (XRD, PANalytical X'Pert Pro MPD diffractometer with Cu radiation) and the micro-

* Electrochemical Society Active Member.
z E-mail: cswang@umd.edu

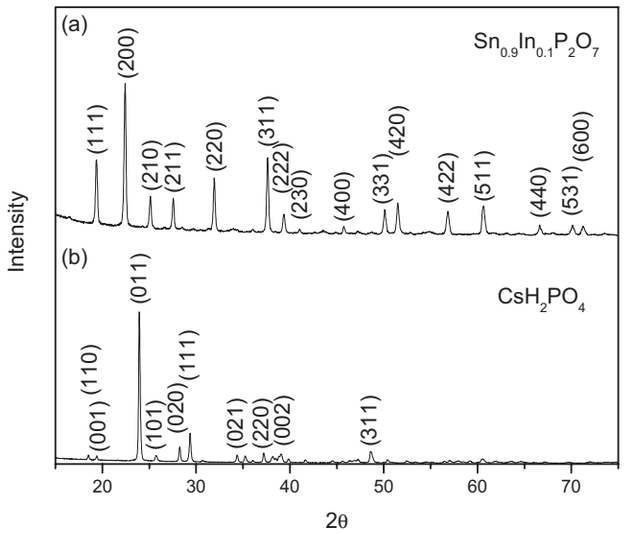

Figure 1. XRD patterns for (a) $Sn_{0.9}In_{0.1}P_2O_7$ and (b) CsH_2PO_4.

morphology of the powders and pellets was observed by scanning electron microscopy images using an FEI Quanta 200 with an electron diffraction spectrometer.

Both the anode and cathode contained two overlapped conductive porous layers: a diffusion layer and a catalyst layer. The diffusion layer was formed from carbon cloth (E-TEK, B1A) which was smoothed by coating a mixture of 85 wt % carbon powder (Vulcan XC72) and 15 wt % poly(tetrafluoroethylene) (PTFE, Aldrich, 60% dispersion). The carbon powder loading was 2 mg/cm^2. The catalyst layer was formed from either $Sn_{0.9}In_{0.1}P_2O_7$ or CsH_2PO_4 (35 wt %), 40 wt % Pt/C catalyst (50 wt %, E-TEK), and PTFE (15 wt %). The catalyst ink was prepared by mixing $Sn_{0.9}In_{0.1}P_2O_7$ (or CsH_2PO_4), distilled water, Pt/C catalyst, isopropanol (Fisher Scientific, 99.9%), and PTFE. The ink was brushed onto the diffusion layer and dried to form an electrode (anode or cathode). The platinum loading was 4 mg/cm^2. The electrolyte membrane ($Sn_{0.9}In_{0.1}P_2O_7$ or CsH_2PO_4) was sandwiched by the anode and cathode to form a single cell. Humidification of gas was achieved by saturating nitrogen/hydrogen/oxygen with water at a given temperature, resulting in a given water partial pressure, such as 76°C for 40% H_2O. To add methanol into fuel gases, hydrogen/nitrogen was saturated with a mixture of methanol and water at a given temperature.

Conductivity measurements were carried out using a Solartron (SI1287 and SI1260) electrochemical impedance system in the frequency range of 0.001–10^6 Hz. At each temperature, the sample was held about 30 min prior to measurement.

Results and Discussion

Figure 1 shows typical XRD patterns for $Sn_{0.9}In_{0.1}P_2O_7$ and CsH_2PO_4 at room temperature. The peaks observed are identical to those reported in PDF# 00-29-1352 (SnP_2O_7) and PDF# 00-35-0746 (CsH_2PO_4). SnP_2O_7 doped with 10% In^{3+} showed the same structure as the undoped SnP_2O_7, characterized by a cubic or pseudocubic structure with SnO_6 octahedral at the corners and P_2O_7 units at the edges.[26] However, Nagao et al. reported that 10% In^{3+} doping increased the lattice constant from 7.945 to 7.950 Å[16] and created oxygen vacancy defects.[14,16] The chemical composition of $Sn_{0.9}In_{0.1}P_2O_7$ was confirmed by energy dispersive analysis by X-rays. All peaks in Fig. 1b could be indexed to CsH_2PO_4, indicating the synthesized material is pure CsH_2PO_4.

Figure 2 shows the morphologies of powders and morphologies of cross sections for $Sn_{0.9}In_{0.1}P_2O_7$ and CsH_2PO_4 pellets. The cross sections were obtained by cutting the pellets with a sharp blade. Although the particle size of $Sn_{0.9}In_{0.1}P_2O_7$ is smaller than that of

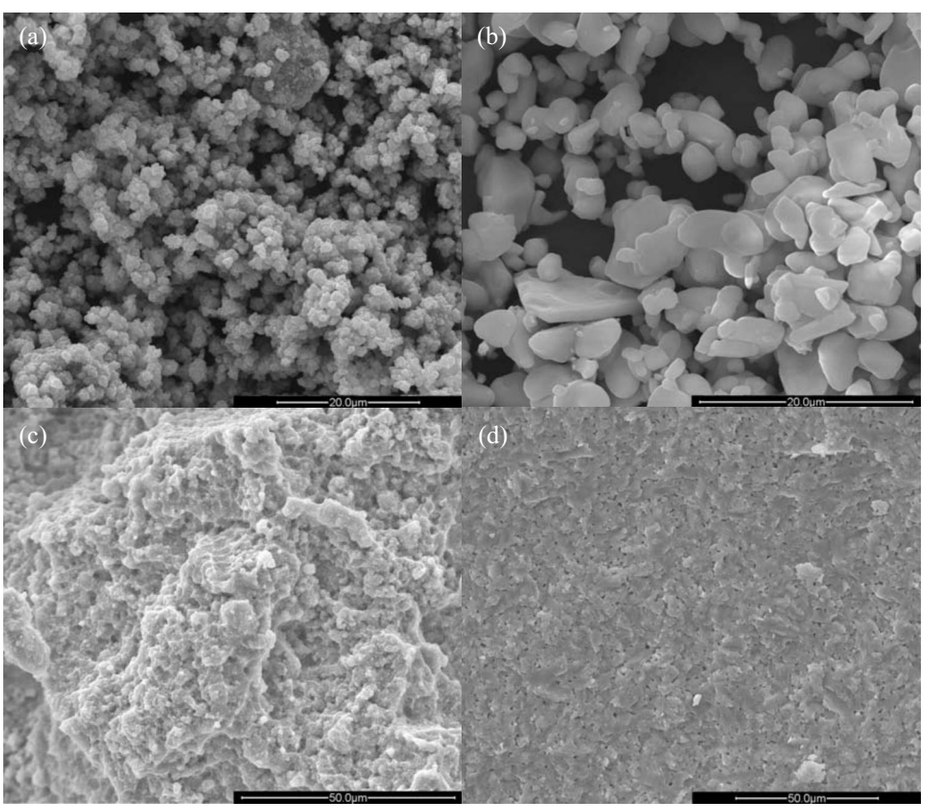

Figure 2. Micromorphologies of (a) $Sn_{0.9}In_{0.1}P_2O_7$ powder, (b) CsH_2PO_4 powder, (c) cross section for $Sn_{0.9}In_{0.1}P_2O_7$ pellet, and (d) cross section for CsH_2PO_4 pellet.

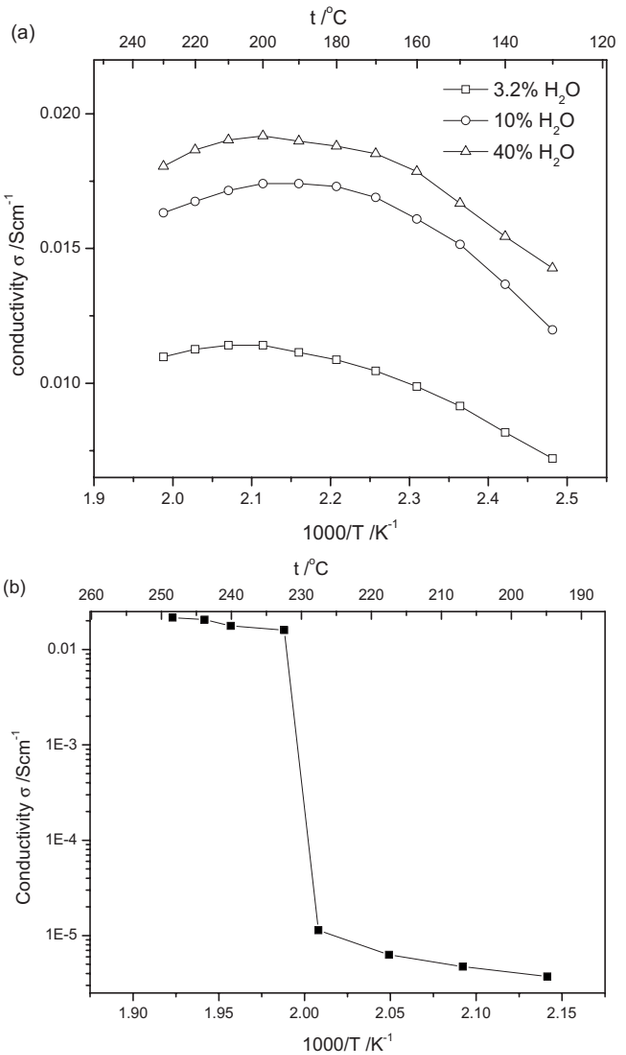

Figure 3. Conductivities of (a) $Sn_{0.9}In_{0.1}P_2O_7$ in wet nitrogen with various water vapor pressures, and (b) CsH_2PO_4 in 40% H_2O/N_2.

CsH_2PO_4, (Fig. 2a and b), the porosity of the former is higher than the latter, i.e., the density of the CsH_2PO_4 pellet is higher than that of $Sn_{0.9}In_{0.1}P_2O_7$ (Fig. 2c and d).

Figure 3 shows the conductivities of $Sn_{0.9}In_{0.1}P_2O_7$ and CsH_2PO_4 at different temperatures in humidified nitrogen. The conductivity of $Sn_{0.9}In_{0.1}P_2O_7$ continuously increased with increasing water vapor pressure from 3.2 to 40% (Fig. 3a). The conduction behavior of $Sn_{0.9}In_{0.1}P_2O_7$ at different temperatures is different from the superprotonic character of CsH_2PO_4, which shows a sharp increase in the conductivity of a few orders of magnitude by a structural transition from a low- to a high-temperature phase (Fig. 3). The maximum protonic conductivities of $Sn_{0.9}In_{0.1}P_2O_7$, achieved at around 200°C in 40% H_2O, is 0.019 S/cm, which is similar to that (0.02 S/cm) of CsH_2PO_4 at 240°C. The thermal variations of proton conductivities for $Sn_{0.9}In_{0.1}P_2O_7$ and CsH_2PO_4 were consistent with reported results,[4,14,27] although the conductivity of $Sn_{0.9}In_{0.1}P_2O_7$ is slightly lower than reported values.[14] The reason why the conductivity decreases after 200°C is not clear. It cannot be attributed to the escape of water produced by the reversal of Reaction 1 because the evolution of water vapor from $Sn_{0.9}In_{0.1}P_2O_7$ starts above 260°C.[16] If it is due to the escape of water, the peak position should not be fixed at 200°C but move to a higher temperature with higher water partial pressure.

The interaction (Reaction 1) between water vapor and oxygen vacancies (and/or electron holes) may be responsible for protonic conduction in $Sn_{0.9}In_{0.1}P_2O_7$,[14,16] which is similar to the mechanism of proton incorporation in perovskite oxides such as $SrCe_{0.95}Yb_{0.05}O_{3-\alpha}$. The increase in conductivity of $Sn_{0.9}In_{0.1}P_2O_7$ with humidity (Fig. 3) supports the hypothesis of the proton conducting mechanism. During the operation of fuel cells, protons generated at the anode (Reaction 2) move through the $Sn_{0.9}In_{0.1}P_2O_7$ membrane to the cathode to react with oxygen (Reaction 3), whereas oxide ions transit in the opposite direction from the cathode (Reaction 4) to the anode to oxidize the CO or CH_3OH (Reaction 5). CO and methanol can also be chemically oxidized with water through a water–gas-shift reaction (Reaction 6) and reforming (Reaction 7) at intermediate temperatures.

Proton conduction in $Sn_{0.9}In_{0.1}P_2O_7$

$$H_2O(g) + V_O^{\bullet\bullet} \rightarrow 2H_i^{\bullet} + O_O^X \left(\text{and/or } H_2O(g) + 2h^{\bullet} \rightarrow 2H_i^{\bullet} + \tfrac{1}{2}O_2\right) \quad [1]$$

Anode reaction in $Sn_{0.9}In_{0.1}P_2O_7$ fuel cells

$$H_2 \rightarrow 2H_i^{\bullet} + 2e^- \quad [2]$$

Cathode reaction in $Sn_{0.9}In_{0.1}P_2O_7$ fuel cells

$$\tfrac{1}{2}O_2 + 2H_i^{\bullet} + 2e^- \rightarrow H_2O \quad [3]$$

Oxide ion conduction in $Sn_{0.9}In_{0.1}P_2O_7$

$$\tfrac{1}{2}O_2 + V_O^{\bullet\bullet} + 2e^- \rightarrow O_O^X \quad [4]$$

Direct CO and methanol oxidation by oxide ion in anode

$$O_O^X + [R] \rightarrow V_O^{\bullet\bullet} + [P] + 2e^- \quad [5]$$

CO oxidation in anode through water–gas-shift reaction

$$H_2O + CO \rightarrow CO_2 + H_2 \quad [6]$$

CH_3OH oxidation in anode through reforming

$$CH_3OH + H_2O \rightarrow CO_2 + 3H_2 \quad [7]$$

Here, $h^{\bullet}$, $H^{\bullet}$, $V_O^{\bullet\bullet}$, $O_O^{\times}$, $[R]$, $[P]$, and e^- denote an electron hole, a proton, an oxygen vacancy, a lattice oxide ion, reductant (CO and CH_3OH), reduction product, and an electron, respectively.

Another possibility for proton conduction in $Sn_{0.9}In_{0.1}P_2O_7$ is the residual phosphoric acid on the surface of material. If phosphoric acid exists on the surface of material, it should be dissolved into water when the $Sn_{0.9}In_{0.1}P_2O_7$ particles are soaked in water; thus, the washed $Sn_{0.9}In_{0.1}P_2O_7$ should have a lower conductivity than that of unwashed $Sn_{0.9}In_{0.1}P_2O_7$. However, the conductivity of washed $Sn_{0.9}In_{0.1}P_2O_7$ shows a similar conductivity with the unwashed one, indicating that proton conductivity in $Sn_{0.9}In_{0.1}P_2O_7$ is mainly through a water–oxygen vacancy reaction. More experiments are still needed to elucidate the exact role of residual phosphoric acid in proton conduction of $Sn_{0.9}In_{0.1}P_2O_7$ if it exists.

To check the conductivity of $Sn_{0.9}In_{0.1}P_2O_7$ electrolyte in fuel cells, the impedances of $Sn_{0.9}In_{0.1}P_2O_7$ membranes were measured in O_2 and N_2 with and without the presence of water (Fig. 4). Compare the impedances of $Sn_{0.9}In_{0.1}P_2O_7$ measured in dry N_2 and dry O_2 (Fig. 4a). The low-frequency line did not intersect the real axis, which indicates that $Sn_{0.9}In_{0.1}P_2O_7$ is an electronic insulator. Adding water to oxygen gas results in an even lower electronic conductivity, as evidenced by an almost straight line in the low-frequency region (Fig. 4b). Figure 4 clearly demonstrates that $Sn_{0.9}In_{0.1}P_2O_7$ is an electronic insulator at temperatures below 200°C whether in a dry or wet atmosphere.

The maximum protonic conductivities of 0.019 S/cm are achieved at around 200°C in 40% H_2O. To avoid the conductivity drop, the $Sn_{0.9}In_{0.1}P_2O_7$ membranes and $Sn_{0.9}In_{0.1}P_2O_7$ fuel cells were tested at 170°C (i.e., below 200°C). Figure 5 shows the time dependence of conductivity of $Sn_{0.9}In_{0.1}P_2O_7$ at 170°C and CsH_2PO_4 at 235°C in wet nitrogen with 40% water vapor. It is clear that the conductivities of both $Sn_{0.9}In_{0.1}P_2O_7$ and CsH_2PO_4 are very

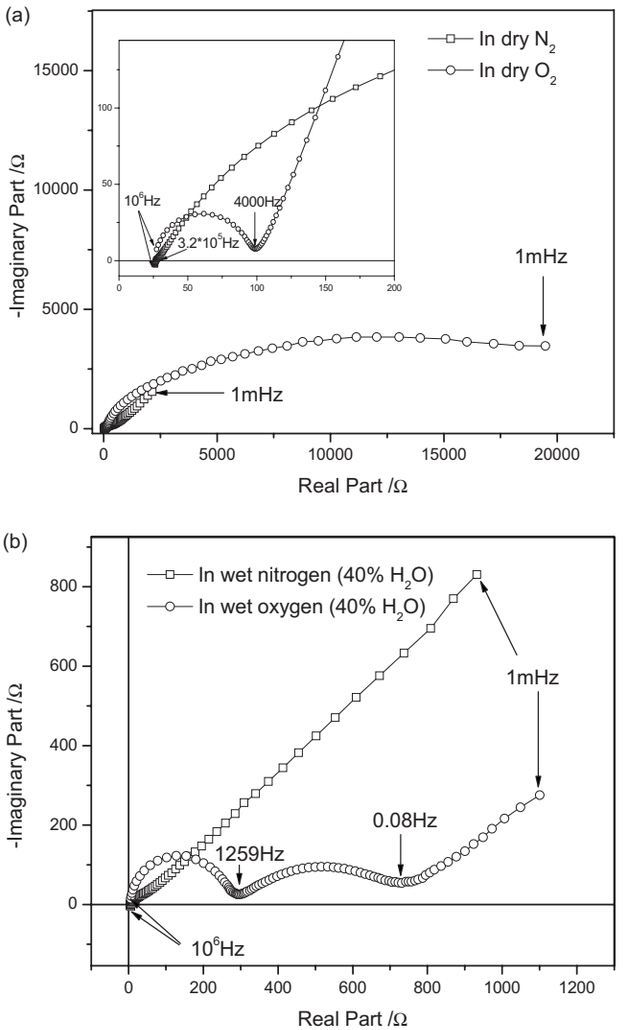

Figure 4. Impedance plots of $Sn_{0.9}In_{0.1}P_2O_7$ in (a) dry and (b) wet condition at 170°C, electrolyte thickness: 0.79 mm for dry oxygen, and 0.80 mm for dry nitrogen, 0.88 mm for wet oxygen, 0.80 mm for wet nitrogen.

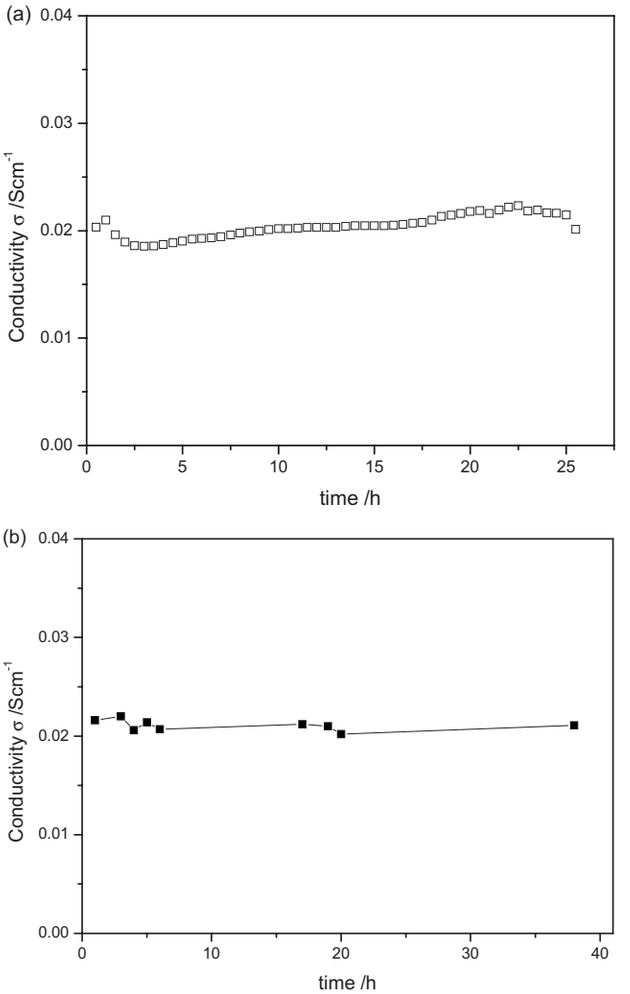

Figure 5. (a) Time dependence of conductivities of $Sn_{0.9}In_{0.1}P_2O_7$ at 170°C in 40% H_2O/N_2 and (b) that of CsH_2PO_4 at 235°C in 40% H_2O/N_2.

stable. Therefore, both $Sn_{0.9}In_{0.1}P_2O_7$ and CsH_2PO_4 are suitable electrolytes for intermediate temperature fuel cells.

Based on Reactions 1 and 4, $Sn_{0.9}In_{0.1}P_2O_7$ should be a mixed proton and oxide ion conductor in humidified gas. In order to confirm $Sn_{0.9}In_{0.1}P_2O_7$ is a mixed-conducting conductor under humidified conditions, the transport numbers of protons and oxide ions were determined by measuring the electromotive force emf of steam concentration cells H_2/O_2 (P_{H_2O} = 0.6 K/Pa), $Pt/C|Sn_{0.9}In_{0.1}P_2O_7|Pt/C$, H_2/O_2 (P_{H_2O} = 3.2 K/Pa). The Nernst potential of the steam concentration cell can be determined by the following equations[28]

$$E_0 = (RT/4F)[t_{ion} \ln(P^{II}_{O_2}/P^{I}_{O_2}) - 2t_{H^+} \ln(P^{II}_{H_2O}/P^{I}_{H_2O})] \quad [8]$$

where $t_{ion} = t_{H^+} + t_{O^{2-}}$ is the ionic transport number and the carrying gas is oxygen. Or

$$E_0 = (RT/2F)[- t_{ion} \ln(P^{II}_{H_2}/P^{I}_{H_2}) + t_{O^{2-}} \ln(P^{II}_{H_2O}/P^{I}_{H_2O})] \quad [9]$$

where the carrying gas is hydrogen.

Because the pressures of the carrying gases (oxygen) at both sides of the steam concentration cell are very close, and the transport number for protons is larger than that for oxide ions (i.e, $2t_{H^+} \gg t_{H^+} + t_{O^{2-}}$), the first parts of Eq. 8 are negligible. Therefore, Eq. 8 can be expressed as $E_0 = -t_{H^+}(RT/2F)\ln(P^{II}_{H_2O}/P^{I}_{H_2O})$, and the proton transport number, t_{H^+}, can be calculated from the measured E_0, $t_{H^+} = E_0/E_{th}$.[29] Here, $E_{th} = (RT/2F)\ln(P^{II}_{H_2O}/P^{I}_{H_2O})$ is defined as the theoretical emf. As shown in Fig. 6a, the proton transport numbers are 0.7–0.8 (average 0.76), depending on the temperatures. After switching the carrying gas from oxygen to hydrogen, the oxygen-ion transport number $t_{O^{2-}}$ at different temperatures can be calculated from Eq. 9 using the measured E_0 values and calculated proton transport numbers at the same temperatures. As shown in Fig. 6b, the oxygen-ion transport numbers are around 0.12. The total ionic transport number (0.88) of $Sn_{0.9}In_{0.1}P_2O_7$ is less than unity, which is probably attributed to gas leakage in the steam concentration cells due to the low density of the membrane (Fig. 2). The gas leakage will result in a lower measured emf than the theoretical value, and less than unity for the total ionic transport numbers. The conductivity of oxide ions in $Sn_{0.9}In_{0.1}P_2O_7$ at 200°C is around 10^{-3} S/cm, which is close to the oxide-ion conductivities of $La_{0.8}Sr_{0.2}Ga_{0.8}Mg_{0.2}$[30] and $Bi_4Ti_{0.2}V_{1.8}O_{10.7}$[31] at 250°C.

The carbon monoxide generated by the reforming reaction would dilute the hydrogen fuel and/or poison the catalyst in the anode even at an intermediate temperature and make the fuel cell performance worse. Because $Sn_{0.9}In_{0.1}P_2O_7$ is a proton and oxide ion co-ion conductor and the oxide ion will oxidize the CO (Reaction 5 can be particularized as $O^X_O + CO \rightarrow V^{\bullet\bullet}_O + CO_2 + 2e^-$), the exhaust CO can become as a fuel in the direct methanol $Sn_{0.9}In_{0.1}P_2O_7$ fuel cells,

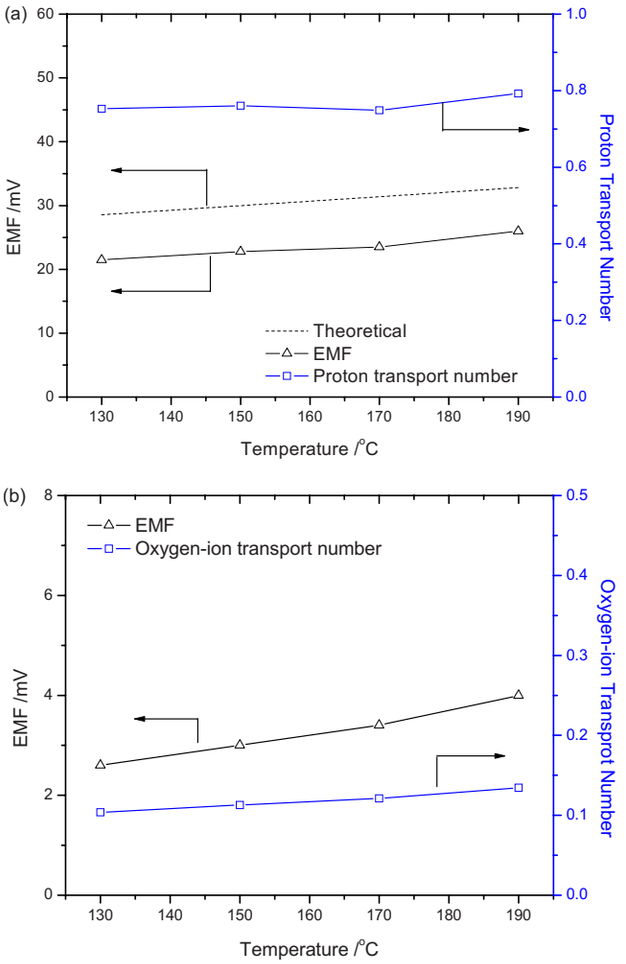

Figure 6. (Color online) The emf values of $Sn_{0.9}In_{0.1}P_2O_7$ membrane galvanic cells at different atmospheres. (a) Anode gas = O_2 (P_{H_2O} = 3.2 kPa); cathode gas = O_2 (P_{H_2O} = 0.6 kPa). (b) Anode gas = H_2 (P_{H_2O} = 0.6 kPa); cathode gas = H_2 (P_{H_2O} = 3.2 kPa); electrolyte thickness: 1.4 mm.

and thus the direct methanol $Sn_{0.9}In_{0.1}P_2O_7$ fuel cells should perform better than direct methanol CsH_2PO_4 fuel cells.

To test the capability of the direct oxidation of CO by oxide ions, the performance of a Pt/C fuel cell using a mixed proton/oxide ion conducting $Sn_{0.9}In_{0.1}P_2O_7$ electrolyte was investigated in the temperature range 130–170°C and compared with a fuel cell using a pure proton conductor CsH_2PO_4 electrolyte at 235°C. Cell voltages and power densities of two cells are shown in Fig. 7 and 8 as a function of current density. As expected, the power density of the $Sn_{0.9}In_{0.1}P_2O_7$ fuel cell increased with temperature and the maximum power densities at 170°C were 14.7 mW/cm^2 for hydrogen, 14.9 mW/cm^2 for a mixture of hydrogen and methanol, and 4.0 mW/cm^2 for methanol. Due to the fast reaction kinetics at a comparatively high operating temperature (235°C) for the CsH_2PO_4 fuel cell, the maximum power density (17.3 mW/cm^2) of the H_2/O_2 CsH_2PO_4 fuel cell was slightly higher than the H_2/O_2 $Sn_{0.9}In_{0.1}P_2O_7$ fuel cell, even though the ionic conductivities of the two electrolytes are very close. However, the power densities of the CsH_2PO_4 fuel cell at 235°C using hydrogen–methanol (13.7 mW/cm^2) and methanol (2.1 mW/cm^2) were much lower than that of the $Sn_{0.9}In_{0.1}P_2O_7$ fuel cell at 170°C. When 15% methanol was added into hydrogen, the power density of the CsH_2PO_4 fuel cell lost 21% power density, decreasing from 17.3 to 13.7 mW/cm^2, but the power density of the $Sn_{0.9}In_{0.1}P_2O_7$ fuel cell remained the same. When the fuel was

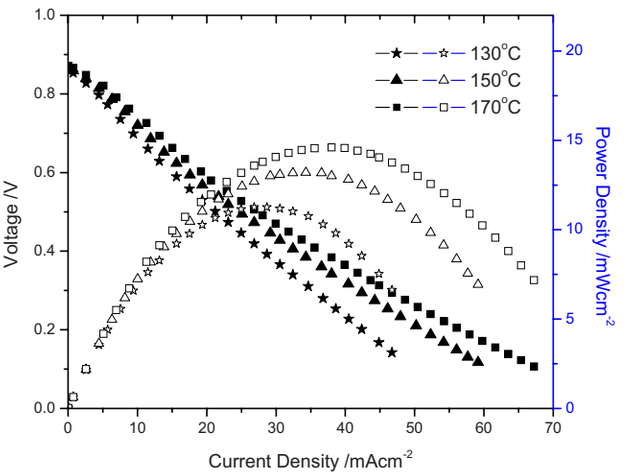

Figure 7. (Color online) Fuel cell performance at different temperature using $Sn_{0.9}In_{0.1}P_2O_7$ as electrolyte and hydrogen as fuel; electrolyte thickness: 0.78 mm.

switched from the H_2–CH_3OH mixture to pure methanol, the power density for the CsH_2PO_4 fuel cell had an 85% drop, from 13.7 to 2.1 mW/cm^2, while the drop for the $Sn_{0.9}In_{0.1}P_2O_7$ fuel cell

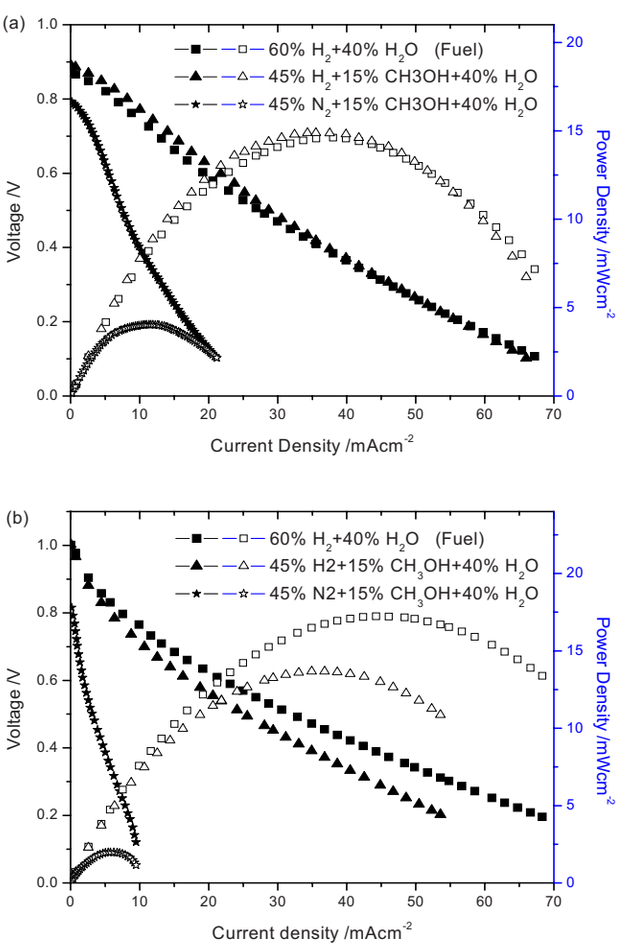

Figure 8. (Color online) Fuel cell performance with various fuels, electrolytes: (a) $Sn_{0.9}In_{0.1}P_2O_7$, thickness: 0.78 mm, 170°C. (b) CsH_2PO_4, thickness: 0.89 mm, 235°C.

was 75%, from 14.9 to 4.0 mW/cm^2. Because both the amount of platinum loading in the two fuel cells and the ionic conductivity of two electrolytes (CsH_2PO_4 and $Sn_{0.9}In_{0.1}P_2O_7$) were the same, even the CsH_2PO_4 cell has a faster electrochemical reaction kinetics than that of the $Sn_{0.9}In_{0.1}P_2O_7$ cell because of its higher operation temperature; the difference in performance must come from the electrolytes. The higher performance of methanol fuel cells using $Sn_{0.9}In_{0.1}P_2O_7$ as an electrolyte at 170°C compared to using a CsH_2PO_4 electrolyte at 235°C strongly indicated that CO was effectively oxidized by the oxide ions, resulting in an enhancement of the fuel cell performance.

Although the CsH_2PO_4 fuel cell has a lower power density than the $Sn_{0.9}In_{0.1}P_2O_7$ fuel cell when methanol is present in the fuel, its open-circuit voltage is higher. This is due to the higher density of the CsH_2PO_4 membrane as shown in Fig. 2, and the higher density may be another reason that the power density of CsH_2PO_4 is higher than $Sn_{0.9}In_{0.1}P_2O_7$ in a H_2/O_2 fuel cell, even though they have very similar conductivities.

Conclusions

A proton and oxide ion co-ion conductor, $Sn_{0.9}In_{0.1}P_2O_7$, was synthesized and characterized. The conductivity of $Sn_{0.9}In_{0.1}P_2O_7$ and performance of $Sn_{0.9}In_{0.1}P_2O_7$ membrane fuel cell were investigated under various atmospheres in the temperature range of 130–230°C and compared with pure proton conductive CsH_2PO_4 and CsH_2PO_4 membrane fuel cells. The conductivity of $Sn_{0.9}In_{0.1}P_2O_7$ reached 0.019 S/cm at 200°C in wet nitrogen, and the transport numbers determined by steam concentration cells were 0.76 for protons and 0.12 for oxide ions. The higher performance of a methanol $Sn_{0.9}In_{0.1}P_2O_7$ fuel cell at 170°C compared to a methanol CsH_2PO_4 fuel cell at 235°C was attributed to the direct oxidation of CO at the anode by the oxide ions transported through the $Sn_{0.9}In_{0.1}P_2O_7$ electrolyte. Due to the unique concept of oxidation of CO by oxide ion transported from the cathode, and preliminary results on a co-ion (proton/oxide ion) conductive fuel cell with methanol fuel, the co-ion conducting membrane fuel cell, operating at around 200°C, may be the next-generation methanol fuel cell and reforming fuel cell because it combines the advantages of both SOFCs and PEMFCs.

Acknowledgment

This material is based upon work supported by the U.S. Army Research Laboratory and the U.S. Army Research Office under grant no. W911NF-06-1-0187. Partial work was done at Tennessee Technological University. The XRD analysis is sponsored by the Assistant Secretary for Energy Efficiency and Renewable Energy, Office of FreedomCAR and Vehicle Technologies, as part of the High Temperature Materials Laboratory User Program, Oak Ridge National Laboratory, managed by UT-Battelle, LLC, for the U.S. Department of Energy under contract no. DE-AC05-00OR22725

University of Maryland assisted in meeting the publication costs of this article.

References

1. T. Norby, *Solid State Ionics*, **125**, 1 (1999).
2. T. Norby, *Nature (London)*, **410**, 877 (2001).
3. S. M. Haile, D. A. Boysen, C. R. I. Chisholm, and R. B. Merle, *Nature (London)*, **410**, 910 (2001).
4. S. M. Haile, C. R. I. Chisholm, K. Sasaki, D. A. Boysen, and T. Uda, *Faraday Discuss.*, **134**, 17 (2007).
5. T. Uda and S. M. Haile, *Electrochem. Solid-State Lett.*, **8**, A245–A246 (2005).
6. D. A. Boysen, T. Uda, C. R. I. Chisholm, and S. M. Haile, *Science*, **303**, 68–70 (2004).
7. T. Uda, D. A. Boysen, C. R. I. Chisholm, and S. M. Haile, *Electrochem. Solid-State Lett.*, **9**, A261 (2006).
8. M. Cappadonia, O. Niemzig, and U. Stimming, *Solid State Ionics*, **125**, 333 (1999).
9. S. Haufe, D. Prochnow, D. Schneider, O. Geier, D. Freude, and U. Stiming, *Solid State Ionics*, **176**, 955 (2005).
10. T. Matsui, S. Takeshita, Y. Iriyama, T. Abe, and Z. Ogumi, *J. Electrochem. Soc.*, **152**, A167 (2005).
11. X. Chen, Z. Huang, and C. Xia, *Solid State Ionics*, **177**, 2413 (2006).
12. X. Chen, X. Li, S. Jiang, C. Xia, and U. Stimming, *Electrochim. Acta*, **51**, 6542 (2006).
13. X. Chen, C. Xia, and U. Stimming, *Electrochim. Acta*, **52**, 7835 (2007).
14. M. Nagao, A. Takeuchi, P. Heo, T. Hibino, M. Sano, and A. Tomita, *Electrochem. Solid-State Lett.*, **9**, A105 (2006).
15. P. Heo, H. Shibata, M. Nagao, T. Hibino, and M. Sano, *J. Electrochem. Soc.*, **153**, A897 (2006).
16. M. Nagao, T. Kamiya, P. Heo, A. Tomita, T. Hibino, and M. Sano, *J. Electrochem. Soc.*, **153**, A1604 (2006).
17. E. P. Murray, T. Tsai, and S. A. Barnett, *Nature (London)*, **400**, 649 (1999).
18. S. Park, J. M. Vohs, and R. J. Gorte, *Nature (London)*, **404**, 265 (2000).
19. P. Mars and D. W. van Krevelen, *Chem. Eng. Sci.*, **3**, 41 (1954).
20. C. Doornkamp and V. Ponec, *J. Mol. Catal. A: Chem.*, **162**, 19 (2000).
21. F. Bertinchamps and E. M. Gaigneaux, *Catal. Today*, **91–91**, 105–110 (2004).
22. H. Over, Y. D. Kim, A. P. Seitsonen, S. Wendt, E. Lundgren, M. Schmid, P. Varga, A. Morgante, and G. Ertl, *Science*, **287**, 1474 (2000).
23. H. Uchida, N. Maeda, and H. Iwahara, *Solid State Ionics*, **11**, 117 (1983).
24. G. Ma, F. Zhang, J. Zhu, and G. Meng, *Chem. Mater.*, **18**, 6006 (2006).
25. B. Zhu, X. Liu, and T. Schober, *Electrochem. Commun.*, **6**, 378 (2004).
26. R. K. B. Gover, N. D. Withers, S. Allen, R. L. Withers, and J. S. O. Evans, *J. Solid State Chem.*, **166**, 42 (2002).
27. J. Otomo, N. Minagawa, C. Wen, K. Eguchi, and H. Takahashi, *Solid State Ionics*, **156**, 357 (2003).
28. J. Guan, S. E. Dorris, U. Balachandran, and M. Liu, *Solid State Ionics*, **100**, 45 (1997).
29. D. P. Sutija, T. Norby, and P. Björnbom, *Solid State Ionics*, **77**, 167 (1995).
30. J. W. Fergus, *J. Power Sources*, **162**, 30 (2006).
31. M. J. Godinho, P. R. Bueno, M. O. Orlandi, and E. Longo, *Mater. Lett.*, **57**, 2540 (2003).